University of Kent

Kent Academic Repository

Urquhart, J. S., Yang, A. Y., Thompson, M. A., König, C, Colombo, D., Kim, W-J, Giannetti, A., Karska, A., Wyrowski, F., Figueira, M. and others (2026) *OGHReS: Discovery of a giant hub-filament system at the edge of the Galactic molecular disc.* Monthly Notices of the Royal Astronomical Society . ISSN 0035-8711.

Downloaded from

https://kar.kent.ac.uk/118104/ The University of Kent's Academic Repository KAR

The version of record is available from

https://doi.org/10.1093/mnras/stag2210

This document version

Publisher pdf

DOI for this version

Licence for this version

CC BY (Attribution)

Additional information

Versions of research works

Versions of Record

If this version is the version of record, it is the same as the published version available on the publisher's web site. Cite as the published version.

Author Accepted Manuscripts

If this document is identified as the Author Accepted Manuscript it is the version after peer review but before type setting, copy editing or publisher branding. Cite as Surname, Initial. (Year) 'Title of article'. To be published in ***Title of Journal*** , Volume and issue numbers [peer-reviewed accepted version]. Available at: DOI or URL (Accessed: date).

Enquiries

If you have questions about this document contact ResearchSupport@kent.ac.uk. Please include the URL of the record in KAR. If you believe that your, or a third party's rights have been compromised through this document please see our Take Down policy (available from https://www.kent.ac.uk/guides/kar-the-kent-academic-repository#policies).

OGHReS: Discovery of a giant hub-filament system at the edge of the Galactic molecular disc*

J. S. Urquhart,[1]†, A. Y. Yang,[2]‡ M. A. Thompson,[3,13] C. König,[4] D. Colombo,[5,4,6,7] W.-J. Kim,[4] A. Giannetti,[8] A. Karska,[9,10] F. Wyrowski,[4] M. Figueira,[11] T. J. T. Moore,[12] L. K. Morgan,[14] Enrique Vázquez-Semadeni,[15]

[1] *Centre for Astrophysics and Planetary Science, University of Kent, Canterbury, CT2 7NH, UK*
[2] *State Key Laboratory of Radio Astronomy and Technology, National Astronomical Observatories, Chinese Academy of Sciences, A20 Datun Road, Chaoyang District, Beijing, 100101, China*
[3] *School of Physics and Astronomy, University of Leeds, Leeds LS2 9JT, UK*
[4] *Max-Planck-Institut für Radioastronomie (MPIfR), Auf dem Hügel 69, 53121 Bonn, Germany*
[5] *Argelander-Institut für Astronomie, Universität Bonn, Auf dem Hügel 71, 53121 Bonn, Germany*
[6] *INAF - Osservatorio Astronomico di Cagliari, Via della Scienza 5, 09047 Selargius (CA), Italy*
[7] *Cluster of Excellence "Our Dynamic Universe" (DYNAVERSE), Institute of Physics I, University of Cologne, Zülpicher Str. 77, 50937 Cologne, Germany*
[8] *INAF - Istituto di Radioastronomia, Via P. Gobetti 101, I-40129 Bologna, Italy*
[9] *Institute of Advanced Studies, Nicolaus Copernicus University in Torun, Wileńska 4, 87-100 Toruń, Poland*
[10] *I Physikalisches Institut, Universität zu Köln, Zülpicher Str. 77, D-50937 Köln, Germany*
[11] *National Centre for Nuclear Research, Pasteura 7, 02-093, Warszawa, Poland*
[12] *Astrophysics Research Institute, Liverpool John Moores University, Liverpool Science Park, 146 Brownlow Hill, Liverpool, L3 5RF, UK*
[13] *INAF - Osservatorio Astrofisico di Catania, Via Santa Sofía 78, I-95123 Catania, Italy*
[14] *NRAO Green Bank Observatory, 155 Observatory Rd, PO Box 2, Green Bank, WV 24944, USA*
[15] *Instituto de Radioastronomía y Astrofísica, Universidad Nacional Autónoma de México, Apdo. postal 3-72, Morelia Mich, 58089, México*

Accepted XXX. Received YYY; in original form ZZZ

ABSTRACT

We present the discovery and characterisation of G195.65−0.10 (also known as the λ-complex), a giant hub-filament system identified by the Outer Galaxy High Resolution Survey (OGHReS). The complex contains 61 spatially and kinematically coherent Hi-GAL clumps with a mean velocity of $V_{\rm LSR} = 32.85\,{\rm km\,s^{-1}}$ and a velocity dispersion between clumps of $1.97\,{\rm km\,s^{-1}}$. A *Gaia* parallax measurement of the central emission-line star MWC 137 associated with an embedded cluster gives a heliocentric distance of $5.2^{+0.8}_{-0.6}$ kpc, placing the complex at a Galactocentric radius of 13.2 kpc. The molecular structure spans approximately 35×63 pc and contains $\sim 1.6 \times 10^5$ M$_\odot$ of molecular gas, including $\sim 5 \times 10^4$ M$_\odot$ in dense clumps. The molecular emission is organised into three prominent velocity-coherent filaments that converge on a dense central hub. Of the associated clumps, 16 are protostellar and 45 are gravitationally bound but currently starless. The protostellar clumps are significantly more concentrated towards the hub than the starless population, with median projected offsets of 6.65 and 15.83 pc, respectively. Moreover, the luminosity-to-mass ratio of the protostellar clumps decreases significantly with increasing distance from the hub, indicating that the most evolutionarily advanced sources are preferentially located in the central region. These results reveal a systematic concentration of dense gas and increasingly evolved star formation towards the hub, with organised large-scale gas motions throughout the filamentary network. The λ-complex therefore provides an unprecedented laboratory to understand hierarchical and high-mass star formation in the outer Galactic disc.

Key words: stars: formation – ISM: clouds – ISM: kinematics and dynamics – Galaxy: structure

1 INTRODUCTION

Filamentary molecular clouds are now recognised as a fundamental component of the Galactic interstellar medium and play a central role in the star formation process. They are observed over a wide range of spatial scales, from giant molecular filaments (GMFs; Li et al. 2013, Ragan et al. 2014; 2015, Abreu-Vicente et al. 2016, Colombo et al. 2021, Mookerjea et al. 2026) extending for hundreds of parsecs and tracing spiral structure, to the dense filamentary networks embedded within giant molecular clouds (André et al. 2014, Inutsuka et al. 2015, Li et al. 2016, Mattern et al. 2018, Schisano et al. 2020). Some of the largest filamentary structures are associated with major segments of spiral arms and have become known as the

* The full version of Table 2 is only available in electronic form at the CDS via anonymous ftp to cdsarc.u-strasbg.fr (130.79.125.5) or via http://cdsweb.u-strasbg.fr/cgi-bin/qcat?J/MNRAS/.

† E-mail: j.s.urquhart@kent.ac.uk
‡ E-mail: yangay@nao.cas.cn

© The Author(s) 2026. Published by Oxford University Press on behalf of Royal Astronomical Society. This is an Open Access article distributed under the terms of the Creative Commons Attribution License (https://creativecommons.org/licenses/by/4.0/), which permits unrestricted reuse, distribution, and reproduction in any medium, provided the original work is properly cited.

ORIGINAL UNEDITED MANUSCRIPT

Downloaded from academic.oup.com/mnras/advance-article/doi/10.1093/mnras/stag2210/9080949 by University of Kent user on 25 November 2026

so-called "bones" of the Milky Way (Goodman et al. 2014, Zucker et al. 2018), emphasising the importance of filaments in defining Galactic structure (see Hacar et al. 2023 for a recent review).

Dense filaments are also intimately linked with star formation. Young stellar objects are preferentially found within filamentary structures (e.g. Lada et al. 2012), while high-mass star formation is frequently concentrated towards dense hubs formed where multiple filaments intersect (Myers 2009, Motte et al. 2018). These hub-filament systems (HFSs) exhibit enhanced concentrations of dense gas, embedded clusters, and massive protostars, and observations increasingly suggest that material is funnelled along the filaments towards the central hub, potentially regulating the formation of stellar clusters and high-mass stars (e.g. Schneider et al. 2012, Mallick et al. 2013, Peretto et al. 2013; 2014, Motte et al. 2018, Williams et al. 2018, Zhou et al. 2022).

Large catalogues of HFSs have recently become available through systematic surveys of the Galactic plane via *Herschel* data. Kumar et al. (2020) identified many thousands of candidate hub-filament systems in the Hi-GAL survey (Elia et al. 2017), demonstrating that approximately 10 per cent of dense Galactic clumps reside within these structures. However, despite their abundance, almost all currently known HFSs are located within the inner Galaxy. Indeed, approximately 98.5 per cent of the Kumar et al. sample lies at Galactocentric radii smaller than the Solar circle ($R_{\rm gc}$ =8.15 kpc; Reid et al. 2019, GRAVITY Collaboration et al. 2019). Only 52 candidates are found in the outer Galaxy and these are all located on the far side of the Galactic disc at heliocentric distances exceeding 20 kpc, making detailed studies of their internal structure extremely difficult. Moreover, these distances are kinematic in nature and therefore likely to be quite uncertain, further complicating the analysis and interpretation of their properties.

The scarcity of well-resolved outer-Galaxy hub-filament systems represents an important limitation for understanding clustered star formation under environmental conditions that differ substantially from those in the inner Milky Way. One of the main reasons for this scarcity is that there has yet to be a systematic search for these systems in the outer Galaxy; Kumar et al. 2020 focused their efforts towards the inner Galaxy Hi-GAL catalogue (Elia et al. 2017) that was available at the time. The outer Galaxy has lower gas surface densities (Heyer et al. 1998), lower metallicities (Lépine et al. 2011, Esteban et al. 2017), weaker spiral perturbations and reduced stellar densities, all of which may influence the formation, evolution and star-forming properties of filamentary molecular clouds. Consequently, it remains unclear whether the hub-filament paradigm established from studies of nearby and inner-Galaxy regions also applies in these more extreme environments.

In this paper we present the discovery and characterisation of G195.65−0.10, a giant hub-filament system identified by the Outer Galaxy High Resolution Survey (OGHReS). Located at a Galactocentric radius of 13.2 kpc (heliocentric distance of 5.15 kpc), the complex is consistent with being associated with the Outer-Norma arm and is one of the most distant well-resolved hub-filament systems currently known. Spanning approximately 35×63 pc, it is considerably larger than the majority of previously studied HFSs, which typically extend over only 10–20 pc (e.g. Kumar et al. 2020; determined from the total length of filaments outside of the central hub), while its relatively nearby heliocentric distance provides a physical resolution several times better than that achieved for currently known outer-Galaxy examples. These characteristics make G195.65−0.10 an exceptional laboratory in which to investigate the relationship between filamentary gas structure and kinematics, clustered and high-mass star formation, and the large-scale environment of the outer Milky Way.

The structure of this paper is as follows. In Sect. 2, we briefly describe the OGHReS survey and introduce G195.65−0.10. Section 3 presents the physical properties of the complex, its molecular gas distribution and star formation characteristics. In Sect. 4, we discuss the implications of these results and compare G195.65−0.10 with other hub–filament systems reported in the literature before summarising our conclusions in Sect. 5.

2 DISCOVERY OF THE λ-COMPLEX

2.1 OGHReS and the identification of molecular complexes

The Outer Galaxy High Resolution Survey (OGHReS; König et al. in prep.) is a systematic high-resolution survey of CO (2–1) emission across approximately 100 deg^2 of the third Galactic quadrant ($180° < \ell < 280°$ and 1° in b), obtained using the Atacama Pathfinder EXperiment (APEX; Güsten et al. 2006) 12 m telescope. The survey provides molecular-line data with an angular resolution of approximately 30 arcsec and a typical sensitivity of $T_{\rm mb} \simeq 0.4$ K per 0.25 km s^{-1} channel, allowing the molecular cloud population of the outer Galaxy to be investigated at a level of detail previously only possible in the inner Galaxy.

In two recent papers, Urquhart et al. (2024; 2025; hereafter Papers I and II), the OGHReS data were used to verify and, where necessary, update the velocities of ∼6 200 Hi-GAL sources (Elia et al. 2021). These velocity measurements were subsequently combined with the projected positions of the clumps in a minimum spanning tree (MST) analysis (see Nešetřil et al. 2001 for a review and Wang et al. 2016 for an application to Galactic star-forming regions). Maximum linking lengths of 6 arcmin and 2 km s^{-1} were adopted in angular position and velocity, respectively, allowing groups of dense clumps that are both spatially and kinematically coherent to be robustly identified. These groups correspond to molecular complexes and filamentary structures that are likely to represent physically connected star-forming regions.

This analysis has identified hundreds of molecular complexes and filamentary structures and the full catalogue will be presented in a forthcoming paper. During inspection of the largest and most significant structures, one complex immediately stood out owing to its exceptional size, organised hub-filament morphology and rich population of dense clumps. This object, centred at $\ell = 195.65°$ and $b = -0.10°$, is the focus of the present paper.

2.2 The G195.65−0.10 Complex

The MST analysis identified a coherent group of 61 Hi-GAL clumps centred at $\ell = 195.72°$, $b = -0.13°$, with a mean velocity of $V_{\rm LSR}$ = 32.85 km s^{-1}. The associated clumps have angular dispersions of $\Delta\ell = 4.7'$ and $\Delta b = 9.4'$, together with an overall velocity dispersion of $\Delta\upsilon = 1.97$ km s^{-1}, indicating that they form a compact, kinematically coherent structure. Inspection of the OGHReS ^{12}CO emission integrated over the same velocity range as the clump reveals that the clumps are embedded within a giant hub-filament system with an extended reservoir of molecular gas that is both spatially and kinematically coherent, confirming that they are part of a single star-forming complex.

The left panel of Figure 1 presents a three-colour image combining the integrated ^{12}CO (2–1), *Herschel* 160 μm and *WISE* 22 μm emission. These wavelengths have been chosen to emphasise the

ORIGINAL UNEDITED MANUSCRIPT

Downloaded from academic.oup.com/mnras/advance-article/doi/10.1093/mnras/stag2210/9080949 by University of Kent user on 25 November 2026

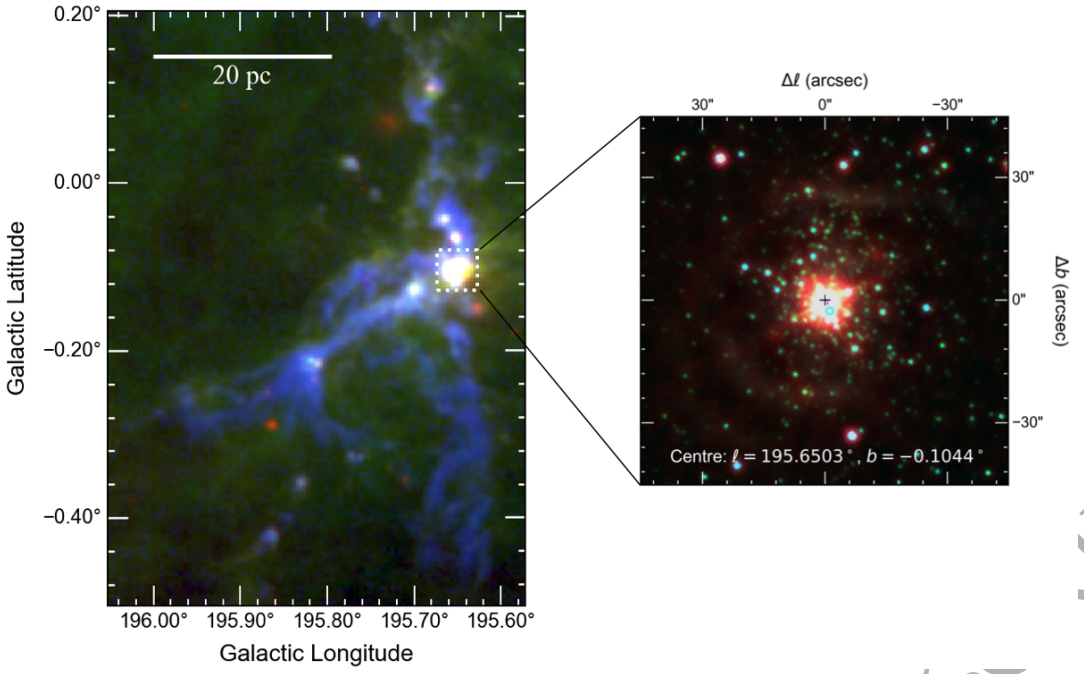

Figure 1. Three-colour composite images of the hub-filament system G195.65−0.10. The image in the left panel has been constructed using the WISE 22 μm (red), the Hi-GAL 160 μm (green) and integrated CO emission (blue); these wavelengths have been selected to contrast the distribution of emission from hot gas, cooler dust emission and cold molecular gas, respectively. The image shown in the right panel is a zoom of the central hub of this complex and is constructed from the UKIDSS J and H band filters (Lawrence et al. 2007; blue and green, respectively) and the 2MASS K_s filter (Skrutskie et al. 2006; red).

distribution of cold molecular gas, cooler dust emission and warm dust associated with embedded star formation. This image reveals the complex to be a highly structured hub-filament system exhibiting significant ongoing star-formation activity. The molecular gas resides in three prominent filaments extending towards the north, south and south-east that converge on a dense central hub. Compact infrared sources are distributed along the filaments, while the hub itself is associated with bright, extended mid-infrared emission indicative of ongoing high-mass star formation.

The central hub is shown in greater detail in the right-hand panel of Fig. 1, which presents a three-colour near-infrared image constructed from the UKIDSS J and H bands (Lawrence et al. 2007) together with the 2MASS K_s band (Skrutskie et al. 2006). This image reveals a compact cluster of bright stars surrounded by diffuse infrared emission offset by approximately 20 arcsec from the geometric centre of the hub. The region has previously been identified with the IRAS source IRAS 06158+1517 ($\ell = 195.6502°$, $b = -0.1046°$), which is associated with the peculiar emission-line star MWC 137 (Kraus et al. 2021). MWC 137 has been classified as a Herbig B[e] supergiant and is surrounded by the optical nebula Sh 2-266 and an embedded infrared cluster (Bica et al. 2003).

The central hub has also been identified as the H II region G195.648−00.106 (Anderson et al. 2015) from analysis of WISE data (Wright et al. 2010). Radio recombination line observations measure a velocity of approximately 28 km s^{-1} (Anderson et al. 2015), which is consistent with both the molecular gas (30.13 km s^{-1}; Wouterloot & Brand 1989) and the velocity of the associated Hi-GAL clumps. A search of the NVSS catalogue (Condon et al. 1998) reveals a coincident 20-cm radio continuum source, NVSS J061845+151652, with an integrated flux density of 93.5 ± 3.5 mJy. At a distance of ∼5 kpc (see Sect. 3.1 for details), this corresponds to a Lyman continuum photon flux of $\log(N_{\rm Ly}) = 47.36$ (Carpenter et al. 1990), consistent with ionisation by an early B-type star corresponding to a $\sim 15\,{\rm M}_\odot$ zero-age main-sequence (ZAMS) star (Davies et al. 2011).

Although the central hub has been studied previously, its association with the extensive molecular filamentary network revealed by OGHReS has not been recognised. We designate the complete structure G195.65−0.10 after the Galactic coordinates of its central hub; however, given its morphological similarity to the Greek letter λ, we also refer to this object as the λ-complex.

3 COMPLEX PROPERTIES

3.1 Distance, mass, size and Galactic location

Using the molecular velocity of 30.13 km s^{-1} measured towards the central IRAS source and the Galactic rotation curve of Brand & Blitz (1993), Wouterloot & Brand (1989) derived Galactocentric and heliocentric distances of $R_{\rm gc}$ =17.76 kpc and D = 9.42 kpc, respectively. Repeating this calculation using the mean velocity of the associated Hi-GAL clumps ($V_{\rm LSR}$ = 32.85 km s^{-1}) together with the updated Galactic rotation parameters of Reid et al. (2019) (R_0 = 8.15 kpc and Θ_0 = 240 km s^{-1}) gives a similar value of $R_{\rm gc}$ =16.46 kpc and D = 8.47 kpc. However, kinematic distances are known to be highly uncertain towards the Galactic anti-centre owing to the shallow velocity gradient in this direction and so these values should be treated with caution.

Fortunately, the central hub contains the emission-line star MWC 137, which is associated with the *Gaia* DR3 source 3344973478481675264. The stellar parallax of this source (0.194 ± 0.0256 mas) corresponds to a heliocentric distance of $D = 5.2^{+0.8}_{-0.6}$ kpc and a Galactocentric distance of $R_{\rm gc}$ =13.2 kpc (Kraus et al. 2021). At this distance, we would expect the complex to have

ORIGINAL UNEDITED MANUSCRIPT

Downloaded from academic.oup.com/mnras/advance-article/doi/10.1093/mnras/stag2210/9080949 by University of Kent user on 25 November 2026

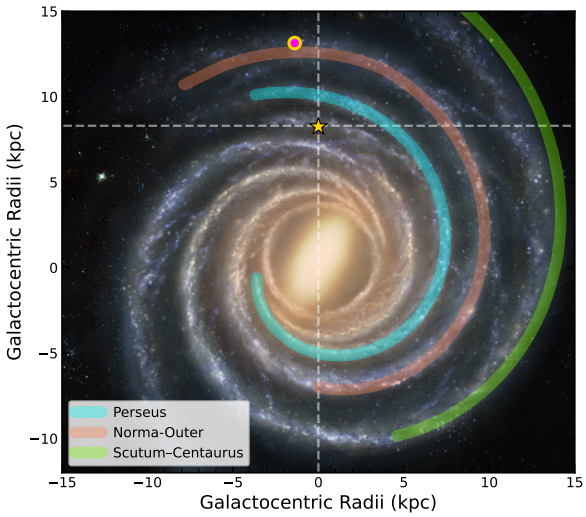

Figure 2. Top-down view of the Milky Way showing the position of the complex determined from the *Gaia* parallax data (filled red circle). The background image is a schematic representation of the Milky Way based on approximately 200 maser parallax measurements (credit: Xing-Wu Zheng & Mark Reid, BeSSeL/NJU/CfA). We highlight the most relevant segments of Perseus, Norma (Reid et al. 2019) and Scutum-Centaurus (Sun et al. 2015; 2024) spiral arms in cyan, red and green respectively. The position of the Sun is shown by the yellow star.

a metallicity approximately $0.4\,Z_\odot$ assuming the radial metallicity gradient (Esteban et al. 2017) and therefore provides a window to study star formation in a very different environment and a link to extragalactic studies. Given the close spatial coincidence between MWC 137, the compact H II region and the centre of the molecular hub, we adopt the *Gaia*-based distance for the entire complex. This distance is consistent with the λ-complex being associated with the Outer-Norma spiral arm as shown in Fig. 2. This also places this complex towards the edge of the Galactic molecular disc ($R_{\rm gc}$ =13.5 kpc; Heyer et al. 1998), making it the most distant high-mass star-forming complex yet discovered with respect to the Galactic centre. Examination of mid-infrared and NVSS radio maps of the extended environment does not reveal any larger scale external features that might have influenced the formation and subsequent evolution of this complex.

The total molecular gas mass of the λ-complex is estimated independently from the integrated ^{12}CO (2–1) emission and the dust-derived H_2 column-density map of Marsh et al. (2015). The spatial extent of the complex was defined using the 2σ contour of the ^{12}CO velocity-integrated intensity map. This mask was applied to both the integrated CO emission and the corresponding Hi-GAL H_2 column-density map to identify the emission associated with the complex (see upper and lower right panels of Fig. 3, respectively).

For the CO data, H_2 column densities were derived from the integrated ^{12}CO (2–1) intensities, $I_{\rm CO\,(2-1)}$, measured from the OGHReS moment-0 map, using:

$$N({\rm H_2}) = X_{\rm CO(1-0)} I_{\rm CO(2-1)} R_{21}^{-1} \left(\frac{Z}{Z_\odot}\right)^{-1.5}, \qquad (1)$$

where $X_{\rm CO(1-0)} = 2.3\times10^{20}$ cm^{-2} (K km s^{-1})$^{-1}$ (Brand & Wouterloot 1995), R_{21} is the CO (1–0) to CO (2–1) line ratio taken as 0.7 (Sandstrom et al. 2013, Nishimura et al. 2015) and $\left(\frac{Z}{Z_\odot}\right)^{-1.5}$ is the correction for the CO-dark gas fraction (Schinnerer & Leroy 2024). The resulting column-density map was integrated over the complex mask assuming a mean molecular weight of $\mu_{\rm H_2} = 2.8$ to give the total mass of the complex of 1.65×10^5 M$_\odot$.

The same spatial mask was applied independently to the dust-derived H_2 column-density map. This gives a total dust mass of the complex as $M_{\rm dust} = 4.0\times10^4$ M$_\odot$ assuming a standard local gas-to-dust ratio of 100 (Elia et al. 2021). However, at the distance of this complex from the Galactic centre ($R_{\rm gc}$ =13.2 kpc) the gas-to-dust ratio is expected to be substantially larger than the local value, reaching approximately 400 (Giannetti et al. 2017) at the distance of this complex. Applying the appropriate Galactocentric-dependent correction increases the estimated total dust derived gas mass to approximately 1.6×10^5 M$_\odot$, which is in excellent agreement with the total mass derived from the CO analysis presented above.

The complex extends approximately 0.4° in Galactic longitude and 0.7° in latitude[1], corresponding to projected physical dimensions of approximately 35×63 pc at the adopted distance of 5.2 kpc. For comparison, most previously identified hub-filament systems have characteristic sizes of approximately 10–20 pc (Kumar et al. 2020). The λ-complex is therefore both substantially larger than a typical HFS and located at a large Galactocentric radius. Its heliocentric distance also provides a physical resolution of approximately 0.75 pc for the 30-arcsec OGHReS beam, considerably better than that available for the most distant outer-Galaxy HFS candidates.

Table 1. Derived filament properties.

Filament designation	Length (pc)	Width (pc)	Aspect ratio	Velocity gradient (km s^{-1} pc^{-1})	ΔV (km s^{-1})
1	41.1	3.1	13.2	-0.01 ± 0.02	···
2	41.8	2.1	19.7	0.18 ± 0.08	7.5
3	33.6	2.2	14.9	0.10 ± 0.02	3.4

3.2 Filamentary structure and kinematics

The morphology of the molecular gas complex is dominated by three extended filamentary structures that converge on the central hub. To quantify their morphology and kinematics, we developed a graph-based analysis combining dendrogram segmentation, skeletonisation and network analysis. The molecular complex was first isolated from the surrounding diffuse emission and reduced to a one-pixel-wide skeleton. The resulting graph representation was then used to identify the principal filamentary spines extending from the central junction and to determine their lengths, widths and aspect ratios.

The three principal structures are shown in the upper right panel of Fig. 3 and are labelled Filaments 1, 2 and 3 (coloured red, blue and green, respectively), and their derived properties are listed in Table 1. They have projected lengths of 41.1, 41.8 and 33.6 pc and characteristic widths of 3.1, 2.1 and 2.2 pc, respectively. Their corresponding aspect ratios range from 13.2 to 19.7, demonstrating that all three structures are highly elongated.

Both the associated Hi-GAL clump velocities and the ^{12}CO moment-1 map reveal a coherent large-scale velocity pattern across the complex (as evidenced by the individual clumps velocities and moment-1 map of the CO gas shown in the upper right and lower

[1] To put this into context, the size of this complex is comparable to the angular size of the full Moon.

ORIGINAL UNEDITED MANUSCRIPT

Downloaded from academic.oup.com/mnras/advance-article/doi/10.1093/mnras/stag2210/9080949 by University of Kent user on 25 November 2026

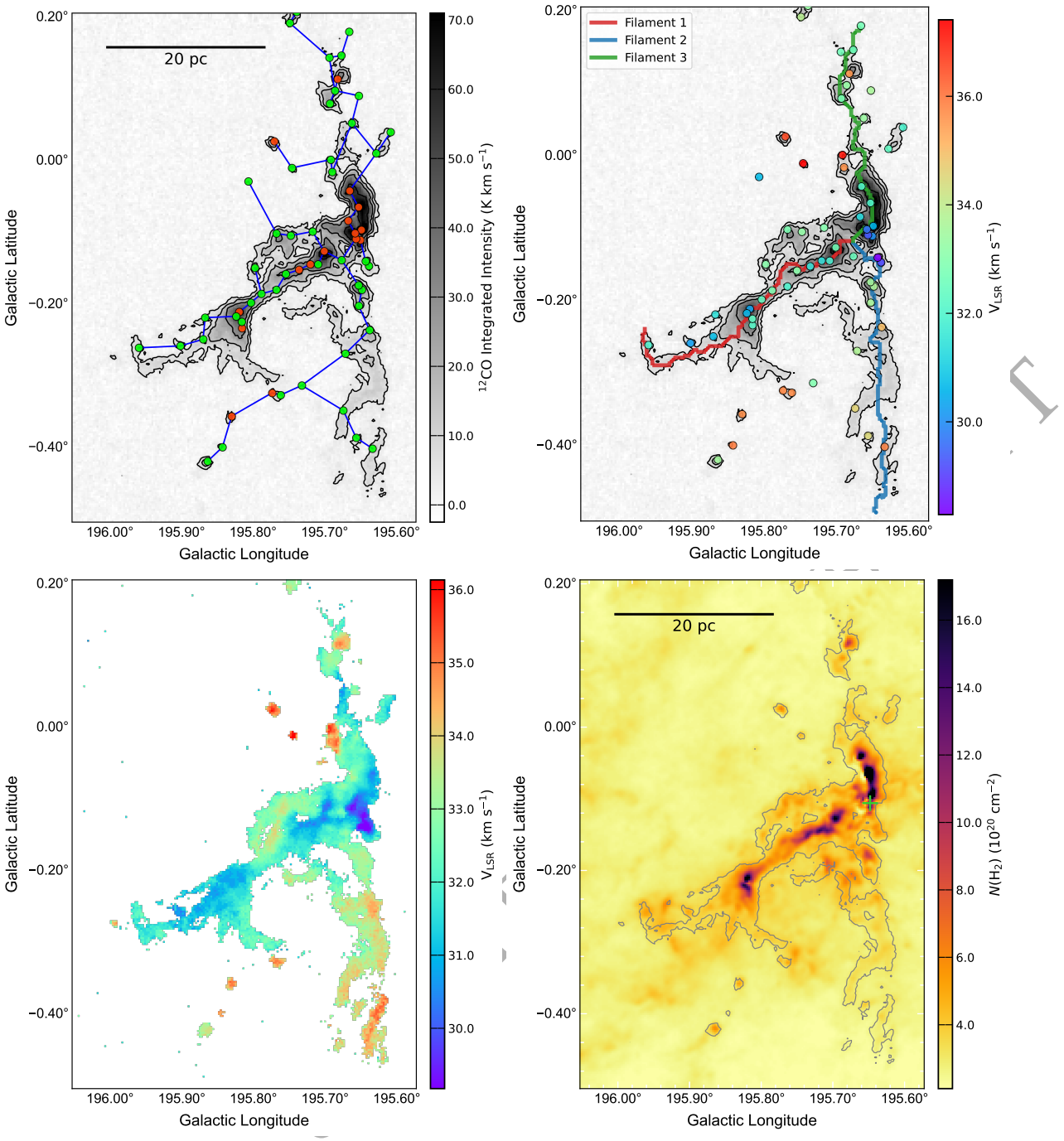

Figure 3. Maps of the λ-complex showing the distribution of different properties or features discussed in the text. The upper panels show the ^{12}CO moment 0 map of the complex (greyscale) with contours starting at 2σ and increasing in steps of 5σ, 10σ, 20σ and 30σ. In the upper left panel, we show the positions of the Hi-GAL clumps that are both kinematically and spatially coincident with the complex; these are coloured according to evolutionary stage (red and green filled circles correspond to protostellar and quiescent bound clumps). The blue connecting lines show the results of the MST analysis. The coloured filled circles shown on the upper right panel also show the positions of associated Hi-GAL clumps but here the colours are linked to the clump velocities (see colour bar for corresponding values). The red, blue and green lines trace the spines of the filaments identified (see Sect. 3.2 for details). In the lower left panel, we show the ^{12}CO moment 1 map, which shows the intensity-weighted mean velocity across the complex. In the lower right panel, we show the column density map produced by Marsh et al. (2015) from the Hi-GAL continuum maps; the contour traces the 2σ level of the integrated ^{12}CO emission shown in the upper panels of this figure.

ORIGINAL

Downloaded from academic.oup.com/mnras/advance-article/doi/10.1093/mnras/stag2210/9080949 by University of Kent user on 25 November 2026

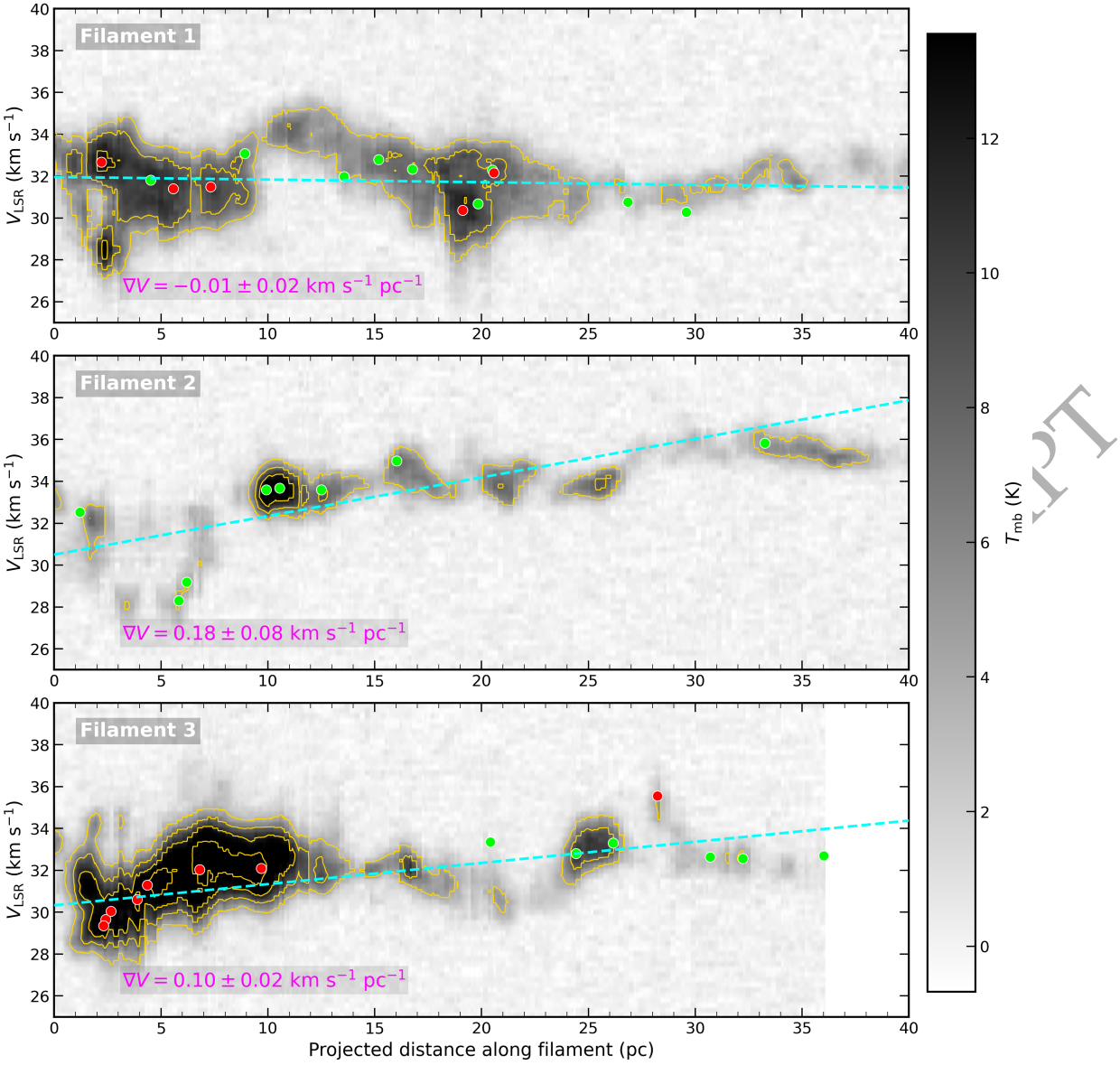

Figure 4. ^{12}CO position-velocity diagrams for the three filaments. The position–velocity cuts begin where the filaments converge and follow their spines (see upper right panel of Fig. 3 for details). The coloured circles indicate the position of protostellar (red) and starless (green) Hi-GAL clumps associated with each filament; which we define as being within a projected distance of 1.5 pc of the filament. The dashed cyan line shows the result of a linear fit to the molecular emission; the fitted velocity gradients are given in the lower-left corner of each panel.

left panels of Fig. 3), with the lowest velocities generally associated with the central hub and increasing velocities towards larger projected distances along the filaments. Superposed on this large-scale pattern are smaller-scale variations associated with individual dense condensations.

To investigate these trends quantitatively, position-velocity cuts were extracted along the three filament spines, beginning at their intersection in the central hub (these are shown in Fig. 4). Linear least-squares fits were used to characterise the variation in velocity with projected distance. The fitted gradients are -0.01 ± 0.02, 0.18 ± 0.08, and 0.10 ± 0.02 km s^{-1} pc^{-1} for Filaments 1, 2 and 3, respectively. These values lie comfortably within the range typically reported for giant molecular filaments (e.g. Ragan et al. 2014). The position-velocity diagrams also show the positions and velocities of the associated Hi-GAL clumps lying within a projected distance of 1.5 pc of each filament spine.

The molecular emission and dense-clump velocities are closely correlated along the filamentary structures. The position-velocity diagrams additionally demonstrate that the protostellar clumps preferentially coincide with the highest-intensity molecular emission, consistent with their association with localised high-column-density regions. Intriguingly, we note the presence of oscillations in the velocity distribution, which have been reported in other regions (e.g., Henshaw et al. 2020, Neupane et al. 2024, He et al. 2026), however, detailed analysis of these features is beyond the scope of the current work.

ORIGINAL UNEDITED MANUSCRIPT

Downloaded from academic.oup.com/mnras/advance-article/doi/10.1093/mnras/stag2210/9080949 by University of Kent user on 25 November 2026

Table 2. Derived clump parameters assuming a heliocentric distance of 5.2 kpc and gas-to-dust ratio of 388.

Hi-GAL name	ℓ (°)	b (°)	Evolution type	T_{dust} (K)	V_{LSR} (km s^{-1})	Σ (g cm^{-2})	$\log_{10}[L_{bol}]$ ($L_\odot$)	$\log_{10}[M_{clump}]$ ($M_\odot$)	L_{bol}/M_{clump}-ratio ($L_\odot/M_\odot$)
HIGALBM195.6079+0.0392	195.6079	0.0392	Starless	11.0	31.94	0.088	1.858	0.424	0.037
HIGALBM195.6280+0.0096	195.6280	0.0096	Starless	11.3	32.35	0.132	2.475	1.202	0.053
HIGALBM195.6332−0.4021	195.6332	−0.4021	Starless	10.0	35.82	0.289	2.189	0.424	0.017
HIGALBM195.6373−0.2367	195.6373	−0.2367	Starless	9.1	34.97	0.378	2.703	0.901	0.016
HIGALBM195.6382−0.1473	195.6382	−0.1473	Starless	8.3	29.18	0.596	3.481	1.424	0.009
HIGALBM195.6429−0.1407	195.6429	−0.1407	Starless	14.3	28.29	0.028	1.490	0.725	0.172
HIGALBM195.6482−0.1806	195.6482	−0.1806	Starless	11.0	33.67	0.358	2.625	1.269	0.044
HIGALBM195.6489−0.0972	195.6488	−0.0972	Protostellar	15.8	30.60	0.615	3.058	3.378	2.092
HIGALBM195.6501−0.1111	195.6501	−0.1111	Protostellar	14.6	30.04	1.059	3.238	3.317	1.200
HIGALBM195.6523+0.0900	195.6523	0.0900	Starless	13.9	33.62	0.047	2.268	1.503	0.172

Notes: Only a small portion of the data is provided here. The full table is available in electronic form at the CDS via anonymous ftp to cdsarc.u-strasbg.fr (130.79.125.5) or via http://cdsweb.u-strasbg.fr/cgi-bin/qcat?J/MNRAS/.

3.3 Dense clumps and star formation

The upper-left panel of Fig. 3 shows the distribution of the associated Hi-GAL clumps over the integrated ^{12}CO (2–1) emission. Protostellar and gravitationally bound starless clumps are indicated by red and green symbols, respectively, while the branches of the MST used to identify the complex are shown in blue. The MST analysis identified 61 Hi-GAL clumps associated spatially and kinematically with the λ-complex. Of these, 16 are classified as protostellar, through their association with a 70-μm point source, while the remaining 45 are classified as gravitationally bound starless clumps (Elia et al. 2021; Urquhart et al. 2025). The resulting star formation fraction, defined as the fraction of Hi-GAL sources with a 70 μm counterpart ($SFF = N_{proto}/N_{all}$; Ragan et al. 2016), is therefore 0.26. This value is similar to that found for star-forming complexes located in the inner Galactic disc (0.25; Ragan et al. 2016), indicating that the star formation activity in this complex is comparable with inner Galaxy complexes.

Although the association of a 70 μm counterpart signifies the presence of an embedded protostellar object, the absence of one does not establish that a clump is starless: a lower-mass or less evolved protostar may be too faint to be detected at this wavelength. Approximately 16 per cent of ATLASGAL clumps classified as starless have been identified as outflow candidates (Urquhart et al. 2022, Yang et al. 2018). If this fraction is representative of the number of starless clumps in the Hi-GAL catalogue, some 70 μm-dark clumps may host protostellar objects, rendering the starless classification less definitive. Molecular outflows are among the earliest signposts of star-formation activity (Urquhart et al. 2022; see their figure 14); an outflow associated with a 70 μm-dark clump is therefore consistent with the embedded protostars being at an earlier evolutionary stage than the 70 μm-bright population. We use the Hi-GAL classifications as useful observational categories, while recognizing that some clumps classified as starless may host early-stage protostars. Although this introduces some uncertainty into the starless sample, the potential number of clumps hosting 70 μm-dark protostars is relatively modest and we do not expect this to significantly affect our results or conclusions.

The physical properties of the clumps (Urquhart et al. 2025) have been rescaled using the adopted *Gaia* distance to the complex and the appropriate gas-to-dust ratio at its Galactocentric radius (Giannetti et al. 2017). The revised surface densities, masses, bolometric luminosities and luminosity-to-mass ratios are listed in Table 2, together with the clump positions, evolutionary classifications, dust temperatures and molecular velocities.

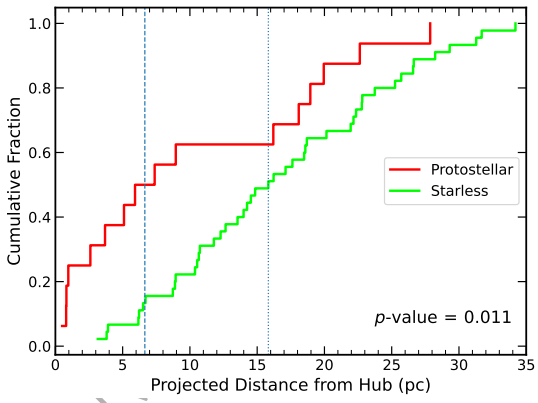

Figure 5. Cumulative distribution function showing the projected distance between protostellar and starless clumps with respect to the centre of the hub. The dotted and dashed vertical lines indicate the median projected distance from the hub of the protostellar and starless clumps respectively. A two-sided Mann-Whitney U test gives p-value = 0.011, indicating that the protostellar and starless clumps have significantly different projected radial distributions.

Summing the individual clump masses gives a total dense-clump mass of approximately $5.0 \times 10^4\,M_\odot$. Comparing this with the total molecular mass of the complex gives a dense-gas fraction of approximately 0.3. This value is larger than the ∼ 0.1 reported in several previous studies of inner Galaxy clump samples (e.g. Eden et al. 2015, Urquhart et al. 2021), however, these studies used the ATLASGAL compact-source catalogue (Contreras et al. 2013), which has a different sensitivity to extended dust emission than Hi-GAL. A direct quantitative comparison should therefore be treated with caution.

Figure 5 shows the cumulative distribution of the projected distance between the protostellar and starless clumps with respect to the central hub. The two populations have noticeably different spatial distributions. Of the 16 protostellar clumps, 10 (63 per cent) are located within 10 pc of the central hub, compared with 24 per cent of the starless population. The most luminous protostellar clumps are also associated with the hub, with the two most luminous sources having $L_{bol} \approx 2 \times 10^3\,L_\odot$, while the total bolometric luminosity obtained by summing the luminosities of the embedded Hi-GAL clumps is approximately $1.2 \times 10^4\,L_\odot$.

The complex contains a substantial population of massive dense clumps, with 18 of the 61 associated Hi-GAL sources having masses

ORIGINAL UNEDITED MANUSCRIPT

Downloaded from academic.oup.com/mnras/advance-article/doi/10.1093/mnras/stag2210/9080949 by University of Kent user on 25 November 2026

exceeding 10^3 M$_\odot$; nine of which are protostellar. Several of the most massive clumps are concentrated within the high-column-density region along Filament 1 and have relatively low $L_{\rm bol}/M_{\rm clump}$, indicating that they are at an early evolutionary stage. A clump mass of 10^3 M$_\odot$ is considered to be the threshold for high-mass star formation[2], and the presence of a significant number of clumps with masses above this threshold may be indicative of ongoing or future high-mass star formation in this complex.

4 DISCUSSION

4.1 A giant hub-filament system in the outer Galactic disc

The λ-complex combines the morphology of a classical hub-filament system with the physical scale of a giant molecular filamentary complex. Its three principal filaments extend for approximately 34–42 pc and converge on a dense central hub, while the full molecular complex spans approximately 35×63 pc. The overall structure of the complex looks strikingly similar to SDC13 (Peretto et al. 2014), although, it is a factor of ten larger in size, and is also substantially larger than the characteristic 10–20 pc dimensions of most hub-filament systems identified by Kumar et al. (2020).

The complex is also unusual in its Galactic location. The adopted Gaia distance places it at $R_{\rm gc}$ =13.2 kpc, making it one of the most distant well-resolved hub-filament systems from the Galactic centre. Kumar et al. (2020) identified only a small number of HFS candidates outside the Solar circle, and these are generally located at much larger heliocentric distances. For example, HF09001 has a reported heliocentric distance of 23.2 kpc (Kumar et al. 2020), corresponding to a physical resolution of approximately 3.4 pc for a 30-arcsec beam. The equivalent physical resolution for the λ-complex is approximately 0.75 pc.

The combination of its large physical extent, substantial molecular reservoir of $\sim 1.6 \times 10^5$ M$_\odot$, and comparatively high physical resolution provides an excellent opportunity to investigate the organisation of dense gas and star formation within a giant HFS in the outer Galactic disc.

4.2 Star formation within the hub-filament system

The spatial distributions of the protostellar and starless clump populations indicate that star formation is not uniformly distributed throughout the complex. Although gravitationally bound starless clumps are found along the full extent of the filamentary network, the protostellar population is preferentially concentrated towards the central hub (Fig. 5). The median projected distance from the hub is 6.65 pc for the protostellar clumps and 15.83 pc for the starless population, and a two-sided Mann-Whitney U test indicates that their radial distributions are significantly different (p-value = 0.011). The contrast is particularly pronounced within the central 10 pc, where 10 of the 20 clumps are protostellar, corresponding to a protostellar fraction of 0.50, compared with only 6 of 41 (0.15) at larger offsets. The central concentration of protostellar clumps therefore appears to be a significant feature of the complex rather than simply a consequence of the particular 10-pc radius adopted for comparison.

[2] This is determined using the relationship between the most massive star in a cluster compared to the embedded cluster mass (i.e. the $m_{\rm max} - M_{\rm ecl}$; Weidner & Kroupa 2006, Weidner et al. 2010) and assuming a typical embedded-cluster star formation efficiency of 30 per cent (Lada & Lada 2003, Wells et al. 2022).

The physical properties of the clumps show a similar radial dependence. Surface density, clump mass and bolometric luminosity all decrease significantly with increasing distance from the hub, with Spearman rank coefficients of $\rho_{\rm S} = -0.36$ (p-value = 0.0044), -0.42 (p-value = 6.8×10^{-4}) and -0.50 (p-value = 4.1×10^{-5}), respectively. The central region therefore preferentially contains the denser, more massive and more luminous clumps in the complex (Fig. 6).

There is also evidence that the protostellar population itself exhibits an evolutionary gradient. As expected, the protostellar clumps have substantially higher luminosity-to-mass ratios than the starless population, with median $L_{\rm bol}/M_{\rm clump}$ values of 0.53 and 0.057 L$_\odot$ M$_\odot^{-1}$, respectively. $L_{\rm bol}/M_{\rm clump}$ provides a commonly used, distance-independent indicator of clump evolution, generally increasing as the luminosity of the embedded stellar population rises relative to the mass of its natal clump (Molinari et al. 2008, Urquhart et al. 2014b). Considering only the 16 protostellar clumps, $L_{\rm bol}/M_{\rm clump}$ decreases significantly with increasing projected distance from the hub ($\rho_{\rm S} = -0.60$, p-value = 0.014; Fig. 7), indicating that the most evolutionarily advanced protostellar clumps are preferentially located towards the central region. A similar, although weaker, trend is seen in dust temperature ($\rho_{\rm S} = -0.47$, p-value = 0.064). Importantly, the $L_{\rm bol}/M_{\rm clump}$-offset relation becomes stronger after controlling for clump mass, with a partial Spearman rank coefficient of $\rho_{\rm partial} = -0.84$. A 10^5-iteration permutation test gives p-value = 1.6×10^{-4}, demonstrating that the observed evolutionary gradient is unlikely to result solely from the preferential concentration of more massive clumps towards the hub. Indeed, many of the most massive clumps are located along the length of Filament 1 away from the central hub.

The concentration of evolved sources towards the hub is particularly significant in the context of high-mass star formation. The central region already contains an embedded stellar cluster, two luminous protostellar clumps associated with candidate high-mass protostellar objects ($L_{\rm bol} > 10^3$ L$_\odot$), and the HII region G195.648−00.106, whose radio continuum emission is consistent with ionisation by a ~ 15 M$_\odot$ ZAMS star (Sect. 2.2). High-mass star formation is therefore already established within the hub. At the same time, 18 of the 61 associated clumps have masses exceeding 10^3 M$_\odot$, demonstrating that a substantial reservoir of massive dense material remains available for further star formation. As previously mentioned, several of the most massive clumps are concentrated within the high-column-density region along Filament 1 and have relatively low $L_{\rm bol}/M_{\rm clump}$ ratios, indicating that they are at an earlier evolutionary stage (see upper and lower left panel of Fig. 6). Thus, while the central hub currently hosts the most evolved and active star formation, the young massive clumps distributed elsewhere in the filamentary network provide considerable potential for future high-mass star formation.

Taken together, these results reveal a clear spatial organisation in both the incidence and evolutionary state of star formation across the λ-complex. The central hub is the current focus of the most advanced star formation, while the surrounding filamentary network contains a substantial reservoir of gravitationally bound and massive clumps at earlier evolutionary stages. The observations do not, however, establish whether this evolutionary segregation results from the dynamical transport of material towards the hub, or whether star formation commenced earlier or proceeds more rapidly there as a consequence of the higher gas and clump densities. Whether the observed spatial and evolutionary organisation is related to material

ORIGINAL UNEDITED MANUSCRIPT

Downloaded from academic.oup.com/mnras/advance-article/doi/10.1093/mnras/stag2210/9080949 by University of Kent user on 25 November 2026

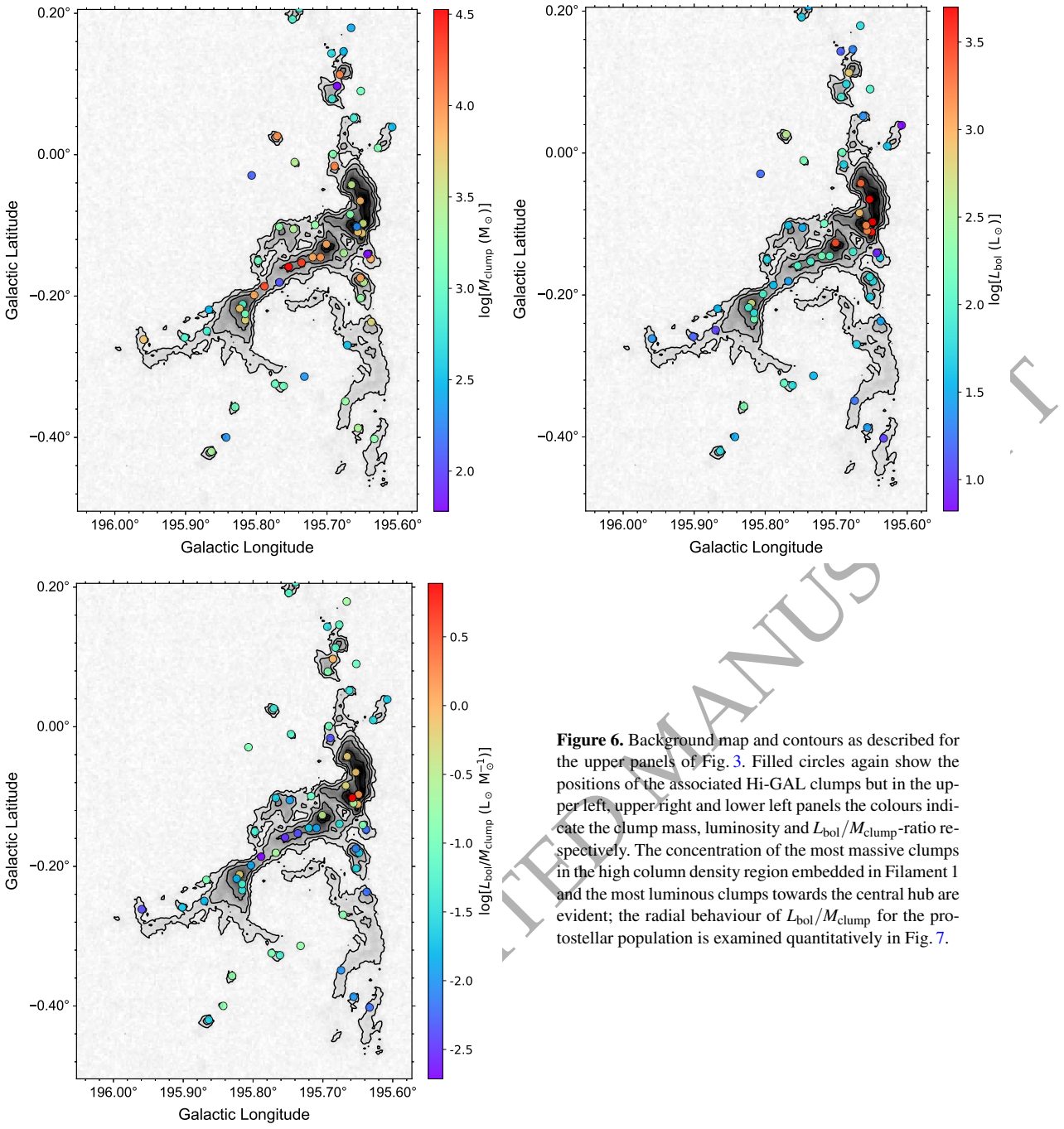

Figure 6. Background map and contours as described for the upper panels of Fig. 3. Filled circles again show the positions of the associated Hi-GAL clumps but in the upper left, upper right and lower left panels the colours indicate the clump mass, luminosity and L_{bol}/M_{clump}-ratio respectively. The concentration of the most massive clumps in the high column density region embedded in Filament 1 and the most luminous clumps towards the central hub are evident; the radial behaviour of L_{bol}/M_{clump} for the protostellar population is examined quantitatively in Fig. 7.

transport through the filamentary network is considered in the following subsection.

4.3 Large-scale gas motions

The clump velocities and the ^{12}CO velocity field reveal coherent large-scale kinematic structure across the complex. In general, the velocity gradients appear steepest near the central hub and become shallower with increasing distance along the filaments. Similar velocity gradients along filaments have been interpreted in other HFSs as evidence for longitudinal gas flows towards central hubs (e.g. Peretto et al. 2014, Williams et al. 2018). In particular, Peretto et al. (2014) found that the gas velocity anti-correlates with velocity dispersion along the SDC13 filaments – the velocity gradients are smaller at the filament ends and increase towards the hub centre – which they attributed to gravitational acceleration along the filaments. The velocity dispersion maximum at the hub centre is naturally explained by the collision of multiple converging flows (Williams et al. 2018). Our CO (2–1) data show a qualitatively similar velocity pattern, although we caution that the optically thick nature of CO (2–1) may introduce additional complexities.

The position-velocity diagrams presented in Fig. 4 provide some support for organised motions along the filaments, but the interpretation is not unambiguous. The fitted gradients differ between the three structures, and the molecular emission exhibits substantial local velocity substructure. In particular, the velocity behaviour along individual filaments is not always well represented by a single linear

ORIGINAL UNCORRECTED MANUSCRIPT

Downloaded from academic.oup.com/mnras/advance-article/doi/10.1093/mnras/stag2210/9080949 by University of Kent user on 25 November 2026

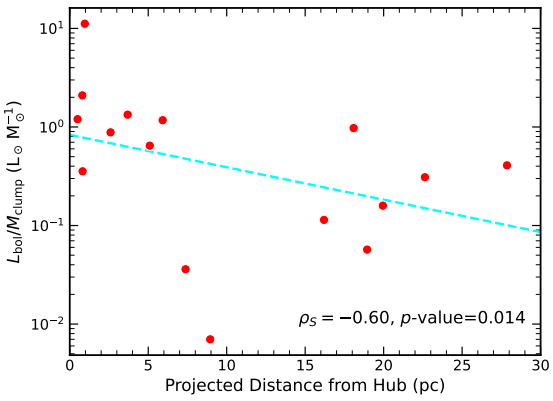

Figure 7. Bolometric luminosity-to-mass ratio of the 16 protostellar Hi-GAL clumps as a function of projected distance from the central hub. The dashed line shows a linear fit to the logarithm of L_{bol}/M_{clump} and is included to illustrate the overall trend. The Spearman rank correlation coefficient and corresponding p-value are given in the lower-right corner.

gradient. The measured line-of-sight gradients are also sensitive to the unknown inclinations of the filaments relative to the plane of the sky.

The observed kinematics are therefore consistent with organised large-scale motions associated with the hub-filament geometry, including the possibility of longitudinal flows towards the hub, but the current observations do not uniquely establish the direction or physical origin of these motions. Alternative contributions from global cloud contraction, local gravitational collapse, projection effects and multiple velocity components cannot presently be excluded.

The coexistence of coherent large-scale velocity structure and smaller-scale kinematic variations associated with individual condensations is qualitatively consistent with hierarchical models of molecular-cloud evolution, in which global contraction and local collapse can occur simultaneously (e.g. Gómez & Vázquez-Semadeni 2014, Vázquez-Semadeni et al. 2009; 2019; 2026, Camacho et al. 2020). Higher spatial and spectral resolution observations using suitable dense-gas tracers will be required to distinguish between these possibilities and to determine whether material is being transported systematically along the filaments towards the central hub.

4.4 Implications for star formation in the outer Galaxy

One of the principal motivations for studying the λ-complex is its location at a Galactocentric radius of 13.2 kpc. Most well-studied hub-filament systems are located considerably closer to the Galactic centre, while the outer Galactic disc is characterised by environmental conditions that differ from those prevailing in the inner Milky Way.

Despite its outer-Galaxy location, this complex exhibits many of the principal characteristics associated with hub-filament systems elsewhere in the Galaxy: multiple elongated molecular structures converge on a high-column-density hub; dense clumps are distributed throughout the filament network; protostellar objects are preferentially concentrated towards the hub; and the molecular gas exhibits coherent velocity structure on scales of several tens of parsecs.

These similarities suggest that the organisation of molecular gas into hub-filament structures and the preferential concentration of star formation towards their intersections can operate efficiently at large Galactocentric radii. The λ-complex therefore provides an important benchmark for investigating whether the physical processes responsible for clustered and high-mass star formation depend strongly on Galactic environment.

The established high-mass star formation within this complex is particularly notable given the declining incidence of high-mass star-forming regions towards the outer Galactic disc (Urquhart et al. 2014a, Djordjevic et al. 2019). This demonstrates that the outer-Galaxy environment is capable not only of producing a giant, highly organised hub-filament system, but also of assembling sufficient dense material to support sustained high-mass star formation (as discussed in Sect. 4.2).

Determining whether the λ-complex is representative of star-forming structures at large Galactocentric radii requires a systematic analysis of the wider OGHReS complex population, which is beyond the scope of the present study.

5 CONCLUSIONS

We have presented the discovery and characterisation of the λ-complex, a giant hub-filament system identified in the OGHReS survey. This complex occupies an unusual region of parameter space. It combines the size of giant filamentary complexes with the morphology of a classical hub-filament system, while lying in one of the most remote star-forming environments yet studied at high spatial resolution. As such it provides an unprecedented laboratory for testing theories of clustered star formation under the lower-metallicity conditions characteristic of the outer Milky Way. Our main conclusions are as follows.

(i) The λ-complex is a spatially and kinematically coherent molecular complex containing 61 Hi-GAL clumps with a mean velocity of $V_{LSR} = 32.85\,km\,s^{-1}$ and a velocity dispersion of $1.97\,km\,s^{-1}$. Adopting the *Gaia* distance of $5.2^{+0.8}_{-0.6}$ kpc to MWC 137, the complex lies at a Galactocentric radius of 13.2 kpc and spans approximately 35×63 pc, making it one of the largest well-resolved hub-filament systems identified in the outer Galactic disc. Furthermore, with a metallicity of $\approx 0.4 Z_\odot$ this complex opens a window to studying HFS and star formation in low-metallicity environments and provides a link to extragalactic star formation studies (e.g. Thilker et al. 2023).

(ii) The molecular emission is organised into three prominent filaments that converge on a dense central hub. The total molecular gas mass is estimated to be $\sim 1.6 \times 10^5\,M_\odot$, while approximately $5 \times 10^4\,M_\odot$ is contained in dense Hi-GAL clumps, corresponding to a dense-gas fraction of ~ 0.3. The individual filaments have lengths of 34-42 pc and widths of 2.1-3.1 pc, giving aspect ratios of 13-20.

(iii) The protostellar population is significantly more concentrated towards the hub than the starless population (median offsets 6.65 versus 15.83 pc; p-value = 0.011). Among the protostellar population, L_{bol}/M_{clump} also decreases significantly with hub offset, and this relation remains significant after controlling for clump mass ($\rho_{partial} = -0.84$, permutation p-value $= 1.6 \times 10^{-4}$).

(iv) The λ-complex is already actively forming high-mass stars while retaining considerable potential for further high-mass star formation. The central hub contains an embedded stellar cluster, two protostellar clumps with $L_{bol} > 10^3\,L_\odot$, and an HII region whose radio continuum emission is consistent with ionisation

ORIGINAL UNEDITED MANUSCRIPT

Downloaded from academic.oup.com/mnras/advance-article/doi/10.1093/mnras/stag2210/9080949 by University of Kent user on 25 November 2026

by a $\sim 15\,M_\odot$ ZAMS star. Moreover, 18 of the 61 associated clumps have masses exceeding $10^3\,M_\odot$, demonstrating that a substantial reservoir of massive dense structures remains distributed throughout the complex. This complex therefore represents not only a giant hub-filament system, but an active high-mass star-forming complex with the potential to sustain further massive-star formation.

(v) The molecular gas exhibits coherent large-scale velocity structure, with velocities generally increasing away from the hub along two of the three principal filaments. These motions are consistent with organised gas flows within the hub-filament network but do not uniquely demonstrate longitudinal accretion. Taken together with the evolutionary segregation of the dense-clump population, the λ-complex provides a particularly well-resolved example of hierarchical and high-mass star formation operating at large Galactocentric radius.

ACKNOWLEDGEMENTS

We thank the referee for their comments and suggestions that have helped clarify a number of aspects of this work. AYY acknowledges the support from the National SKA Program of China (2025SKA0140100), and National Natural Science Foundation of China (NSFC) grants No. 12303031. MAT acknowledges support from STFC grant awards ST/R000905/1 and ST/W00125X/1. DC acknowledges support from the Deutsche Forschungsgemeinschaft (DFG; German Research Foundation) through Collaborative Research Centre SFB 1601 (subproject B3; grant No. 500700252) and Germany's Excellence Strategy, EXC 3037 "Our Dynamic Universe" (grant No. 533607693). AK and MF acknowledge support from the Polish National Science Center SONATA BIS grant No. 2024/54/E/ST9/00314 and SONATA grant No. 2022/47/D/ST9/00419 respectively.

DATA AVAILABILITY

The Hi-GAL catalogue used for this work can be found at http://vialactea.iaps.inaf.it/vialactea/public/ and the OGHReS catalogue used here can be found on CDS.

REFERENCES

Abreu-Vicente J., Ragan S., Kainulainen J., Henning T., Beuther H., Johnston K., 2016, A&A, 590, A131
Anderson L. D., Armentrout W. P., Johnstone B. M., Bania T. M., Balser D. S., Wenger T. V., Cunningham V., 2015, ApJS, 221, 26
André P., Di Francesco J., Ward-Thompson D., Inutsuka S.-I., Pudritz R. E., Pineda J. E., 2014, in Beuther H., Klessen R. S., Dullemond C. P., Henning T., eds, Protostars and Planets VI. pp 27–51 (arXiv:1312.6232), doi:10.2458/azu_uapress_9780816531240-ch002
Bica E., Dutra C. M., Barbuy B., 2003, A&A, 397, 177
Brand J., Blitz L., 1993, A&A, 275, 67
Brand J., Wouterloot J. G. A., 1995, A&A, 303, 851
Camacho V., Vázquez-Semadeni E., Palau A., Busquet G., Zamora-Avilés M., 2020, ApJ, 903, 46
Carpenter J. M., Snell R. L., Schloerb F. P., 1990, ApJ, 362, 147
Colombo D., et al., 2021, A&A, 655, L2
Condon J. J., Cotton W. D., Greisen E. W., Yin Q. F., Perley R. A., Taylor G. B., Broderick J. J., 1998, AJ, 115, 1693
Contreras Y., et al., 2013, A&A, 549, A45
Davies B., Hoare M. G., Lumsden S. L., Hosokawa T., Oudmaijer R. D., Urquhart J. S., Mottram J. C., Stead J., 2011, MNRAS, 416, 972
Djordjevic J. O., Thompson M. A., Urquhart J. S., Forbrich J., 2019, MNRAS, 487, 1057
Eden D. J., Moore T. J. T., Urquhart J. S., Elia D., Plume R., Rigby A. J., Thompson M. A., 2015, MNRAS, 452, 289
Elia D., et al., 2017, MNRAS, 471, 100
Elia D., et al., 2021, MNRAS, 504, 2742
Esteban C., Fang X., García-Rojas J., Toribio San Cipriano L., 2017, MNRAS, 471, 987
GRAVITY Collaboration et al., 2019, A&A, 625, L10
Giannetti A., et al., 2017, A&A, 606, L12
Gómez G. C., Vázquez-Semadeni E., 2014, ApJ, 791, 124
Goodman A. A., et al., 2014, ApJ, 797, 53
Güsten R., Nyman L. Å., Schilke P., Menten K., Cesarsky C., Booth R., 2006, A&A, 454, L13
Hacar A., Clark S. E., Heitsch F., Kainulainen J., Panopoulou G. V., Seifried D., Smith R., 2023, in Inutsuka S., Aikawa Y., Muto T., Tomida K., Tamura M., eds, Astronomical Society of the Pacific Conference Series Vol. 534, Protostars and Planets VII. p. 153 (arXiv:2203.09562), doi:10.48550/arXiv.2203.09562
He Q.-R., et al., 2026, AJ, 171, 234
Henshaw J. D., et al., 2020, Nature Astronomy, 4, 1064
Heyer M. H., Brunt C., Snell R. L., Howe J. E., Schloerb F. P., Carpenter J. M., 1998, ApJS, 115, 241
Inutsuka S.-i., Inoue T., Iwasaki K., Hosokawa T., 2015, A&A, 580, A49
Kraus M., Liimets T., Moiseev A., Sánchez Arias J. P., Nickeler D. H., Cidale L. S., Jones D., 2021, AJ, 162, 150
Kumar M. S. N., Palmeirim P., Arzoumanian D., Inutsuka S. I., 2020, A&A, 642, A87
Lada C. J., Lada E. A., 2003, ARA&A, 41, 57
Lada C. J., Forbrich J., Lombardi M., Alves J. F., 2012, ApJ, 745, 190
Lawrence A., et al., 2007, MNRAS, 379, 1599
Lépine J. R. D., et al., 2011, MNRAS, 417, 698
Li G.-X., Wyrowski F., Menten K., Belloche A., 2013, A&A, 559, A34
Li G.-X., Urquhart J. S., Leurini S., Csengeri T., Wyrowski F., Menten K. M., Schuller F., 2016, A&A, 591, A5
Mallick K. K., Kumar M. S. N., Ojha D. K., Bachiller R., Samal M. R., Pirogov L., 2013, ApJ, 779, 113
Marsh K. A., Whitworth A. P., Lomax O., 2015, MNRAS, 454, 4282
Mattern M., et al., 2018, A&A, 619, A166
Molinari S., Pezzuto S., Cesaroni R., Brand J., Faustini F., Testi L., 2008, A&A, 481, 345
Mookerjea B., Sen S., Veena V. S., Kramer C., 2026, A&A, 706, A287
Motte F., Bontemps S., Louvet F., 2018, ARA&A, 56, 41
Myers P. C., 2009, ApJ, 700, 1609
Neupane S., Wyrowski F., Menten K. M., Urquhart J., Colombo D., Lin L.-H., Garay G., 2024, A&A, 692, A114
Nešetřil J., Milková E., Nešetřilová H., 2001, Discrete Mathematics, 233, 3
Nishimura A., et al., 2015, ApJS, 216, 18
Peretto N., et al., 2013, A&A, 555, A112
Peretto N., et al., 2014, A&A, 561, A83
Ragan S. E., Henning T., Tackenberg J., Beuther H., Johnston K. G., Kainulainen J., Linz H., 2014, A&A, 568, A73
Ragan S. E., Henning T., Beuther H., Linz H., Zahorecz S., 2015, A&A, 573, A119
Ragan S. E., Moore T. J. T., Eden D. J., Hoare M. G., Elia D., Molinari S., 2016, MNRAS, 462, 3123
Reid M. J., et al., 2019, ApJ, 885, 131
Sandstrom K. M., et al., 2013, ApJ, 777, 5
Schinnerer E., Leroy A. K., 2024, ARA&A, 62, 369
Schisano E., et al., 2020, MNRAS, 492, 5420
Schneider N., et al., 2012, A&A, 540, L11
Skrutskie M. F., et al., 2006, AJ, 131, 1163
Sun Y., Xu Y., Yang J., Li F.-C., Du X.-Y., Zhang S.-B., Zhou X., 2015, ApJ, 798, L27
Sun Y., et al., 2024, ApJ, 977, L35
Thilker D. A., et al., 2023, ApJ, 944, L13

ORIGINAL UNEDITED MANUSCRIPT

Downloaded from academic.oup.com/mnras/advance-article/doi/10.1093/mnras/stag2210/9080949 by University of Kent user on 25 November 2026

Urquhart J. S., Figura C. C., Moore T. J. T., Hoare M. G., Lumsden S. L., Mottram J. C., Thompson M. A., Oudmaijer R. D., 2014a, MNRAS, 437, 1791
Urquhart J. S., et al., 2014b, MNRAS, 443, 1555
Urquhart J. S., et al., 2021, MNRAS, 500, 3050
Urquhart J. S., et al., 2022, MNRAS, 510, 3389
Urquhart J. S., et al., 2024, MNRAS, 528, 4746
Urquhart J. S., et al., 2025, MNRAS, 539, 3105
Vázquez-Semadeni E., Gómez G. C., Jappsen A.-K., Ballesteros-Paredes J., Klessen R. S., 2009, ApJ, 707, 1023
Vázquez-Semadeni E., Palau A., Ballesteros-Paredes J., Gómez G. C., Zamora-Avilés M., 2019, MNRAS, 490, 3061
Vázquez-Semadeni E., et al., 2026, MNRAS, 547, 2059
Wang K., Testi L., Burkert A., Walmsley C. M., Beuther H., Henning T., 2016, ApJS, 226, 9
Weidner C., Kroupa P., 2006, MNRAS, 365, 1333
Weidner C., Kroupa P., Bonnell I. A. D., 2010, MNRAS, 401, 275
Wells M. R. A., Urquhart J. S., Moore T. J. T., Browning K. E., Ragan S. E., Rigby A. J., Eden D. J., Thompson M. A., 2022, MNRAS, 516, 4245
Williams G. M., Peretto N., Avison A., Duarte-Cabral A., Fuller G. A., 2018, A&A, 613, A11
Wouterloot J. G. A., Brand J., 1989, A&AS, 80, 149
Wright E. L., et al., 2010, AJ, 140, 1868
Yang A. Y., Thompson M. A., Urquhart J. S., Tian W. W., 2018, ApJS, 235, 3
Zhou J.-W., et al., 2022, MNRAS, 514, 6038
Zucker C., Battersby C., Goodman A., 2018, ApJ, 864, 153

ORIGINAL UNEDITED MANUSCRIPT

Downloaded from academic.oup.com/mnras/advance-article/doi/10.1093/mnras/stag2210/9080949 by University of Kent user on 25 November 2026